Direct depth imaging without a velocity model: update and Marmousi model tests

Fang Liu and Arthur B. Weglein, Mission-Oriented Seismic Research Program, University of Houston

SUMMARY

The inverse scattering subseries for direct depth imaging without a velocity model has demonstrated its viability on synthetic and field data. The current direct depth imaging algorithm is: (1) closed form and very fast, and (2) represents only a very small portion of the depth imaging terms/capability within the inverse scattering (ISS) series. In this paper, we demonstrated the effectiveness of the current depth imaging algorithm on the Marmousi data set. Equally important, we witness the promise and potential of direct depth imaging algorithm from the inverse scattering series and its moving closer to belonging in our seismic depth imaging toolbox, taking its place alongside its siblings for free surface and internal multiple removal.

THEORY

In the inverse scattering series (Weglein et al., 2000, 2002), the perturbation α is defined as the difference between the actual and reference velocity: $\frac{1}{c^2}=\frac{1}{c_0^2}(1-\alpha)$, where c is the spatially varying actual velocity, c_0 (in this example just homogeneous water velocity for the entire space) is the reference velocity. In 2D, both α and c are functions of depth z and lateral variable x. The perturbation α is separated into an infinite series in terms of their order of dependence in terms of the data at the measurement surface:

$$\alpha(x,z)=\alpha_1+\alpha_2+\alpha_3+\cdots \tag{1}$$

where the first term α_1 is essentially equivalent to prestack FK migration.

$$\begin{aligned}\alpha_1(k_m,k_z,\theta)&=-4\frac{q_g q_s}{\omega^2/c_0^2}D(k_m,k_z,\omega),\\ \omega&=\frac{c_0 k_z}{2}\sqrt{\frac{k_z^2+k_m^2}{k_z^2\cos^2\theta-k_m^2\sin^2\theta}}.\end{aligned} \tag{2}$$

Seismic data, originally a function of time t, x_s (source lateral coordinate) and x_g (receiver lateral coordinate), are sorted into x_m (mid-point) and x_h (offset) domain, and are then Fourier transformed into k_m (the Fourier conjugate of x_m), k_h (the Fourier conjugate of x_h) and ω (temporal frequency) domain to compute the data D in the right-hand-side of equation (2). In the calculation, we choose $k_m=k_g-k_s$, $k_h=k_g+k_s=2\sin\theta\omega/c_0$. And equation (2) can be Fourier transformed from k_m to x, and k_z to z to have α_1 in the spatial (x,z) domain. Note that although α is not a function of the parameter θ, its Born approximation α_1 is. This is the reason why specular reflections are not flat in the angle (or common-image) gather domain, in other words, are imaged at different depth for different angles θ, when employing a constant velocity FK migration.

The second term α_2 can be computed from the first term α_1 as:

$$\alpha_2(x,z)=\alpha_{21}+\alpha_{22}+\alpha_{23}, \tag{3}$$

where its first two terms are:

$$\begin{aligned}\alpha_{21}&=-\frac{\alpha_1^2(x,z)}{2}-\frac{\partial\alpha_1(x,z)}{2\partial z}\int_{-\infty}^{z}\alpha_1(x,z')dz',\\ \alpha_{22}&=\frac{\partial\alpha_1(x,z)}{2\partial x}\int_{-\infty}^{z}dz'\int_{-\infty}^{z'}dz''\frac{\partial\alpha_1(x,z'')}{\partial x}.\end{aligned} \tag{4}$$

And the third term is expressed in the k domain as:

$$\begin{aligned}\widetilde{\alpha}_{23}(k,z)=\frac{1}{8\pi^2}\int_{-\infty}^{\infty}\widetilde{\alpha}_1(\frac{k}{2}-k',z')\int_{-\infty}^{z'}\widetilde{\alpha}_1(\frac{k}{2}+k',z'')\\ \times\widetilde{\xi}_2\left(k,k',\frac{z'+z''}{2}-z,\frac{z'-z''}{2}\right)dz'dz'',\end{aligned} \tag{5}$$

where $\widetilde{\xi}_2(k,k',\varepsilon_0,\varepsilon_1)=\int_{-\infty}^{\infty}e^{i(\varepsilon_0+\varepsilon_1)k_z}(i(k_z^2+k_m^2)/(u_1)e^{i\Delta\psi}-ik_z+\varepsilon_1 a_1/2)$, $a_1=k^2-4k'^2$, $u_1=\sqrt{k_z^2+a_1}$, $\Delta\psi=\varepsilon_1(u_1-k_z)$.

So far the second term of α_{21} (the only term in α_2 that does not vanish if the earth has no lateral variation) has been incorporated into the leading-order imaging subseries (LOIS) (Shaw, 2005) and higher-order imaging subseries (HOIS). The other two terms α_{22} and α_{23} will vanish if the earth does not vary laterally, in other words, laterally exclusive (LE) terms.

$$\alpha^{\texttt{LOIS}}(x,z)=\alpha_1\left(x,z-\frac{1}{2}\int_{-\infty}^{z}\alpha_1(x,z')dz'\right), \tag{6}$$

$$\alpha^{\texttt{HOIS}}(x,z+\frac{1}{2}\int_{-\infty}^{z}dz'\frac{\alpha_1(x,z')}{\cos^2\theta-\frac{\alpha_1(x,z')}{4}})=\alpha_1(x,z). \tag{7}$$

Both LOIS and HOIS are task-specific subseries for seismic imaging and aim to further migrate primaries in α_1 to their actual location without updating the migration velocity c_0. If the imaging subseries has achieved the actual depth of a reflector, which is independent of the angle θ, the reflector image

should be migrated to the same depth for all angles, or in other words, flattened. This is how can the flatness of events in the angle gather be used as a benchmark for the effectiveness of our algorithm, although the flatness of events does not enter the procedure anywhere.

THE MARMOUSI MODEL AND OUR FINITE-DIFFERENCE MODELING PROCEDURE

The Marmousi model is one of the well know benchmark seismic imaging challenges. The original model is sampled every $1.25(m)$ in both the vertical and the horizontal directions. In the modeling procedure we resample it at $5(m)$ and boost the the wave speed of a low velocity region to water velocity ($1500m/s$) to accomodate the coarser $5(m)$ sampling. In the framework set up in Weglein et al. (2000, 2002), α_1 is the first term in the seismic imaging subseries and is essentially equivalent to a prestack Stolt migration with constant velocity. In this note, α_1 (the first term of inverse scattering series) and the subsequent higher-order imaging subseries are shown. For this model with very big velocity contrast (the highest velocity being $4700m/s$ vs the reference $1500m/s$ water speed) and large lateral variation, the idea of purposeful perturbation (see Weglein (2006) for detail) observed in all previous simpler imaging challenges still holds for the much more complicated Marmousi model.

There are hundreds of reflectors (horizons) in the Marmousi model, to display all of them at the same time will block a significant portion of the data. Therefore in each figure we selected only the major reflectors for display.

The original Marmousi model (see Figure 1) has a small region of very low velocity. Since the wavelength of seismic wave is shorter in the low velocity zone, the extreme low velocity requires very fine sampling in both the x and z directions. Since this low velocity zone is located in the portion of the model with very mild lateral variation, the low velocity contrast by itself (without large lateral variation) was not a major challenge for HOIS. This modification (shown in Figure 2) does not reduce the imaging challenge for our direct depth imaging.

In the finite difference modeling procedure, the interval between two adjacent time step is $0.5ms$, but the sampling interval in the output is $2ms$ to follow the standard choice in seismic data. A typical shot gather is shown in Figure 3. In the modeling procedure, only the P-wave velocity is used.

The wavelet used in the finite-difference procedure is the first derivative of a Gaussian function, lacking zero frequency information. Just as our previous numerical examples in Liu (2006) and real data example in Weglein et al. (2012), low frequency is not an issue. Limited aperture, or lack of data, often seriously compromise a lateral Fourier transform, and evaporize the inherent logic between seismic events that crystalizes in the k-domain, just as shown in internal multiple attenuation examples.

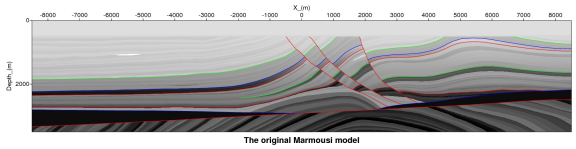

Figure 1: The original Marmousi model. The wave speed of the low velocity region in this model (shown by the bright zone with x-coordinate between $-6000(m)$ and $-5000(m)$) will be boosted to water speed ($1500m/s$). The colored horizons are major reflectors in the model.

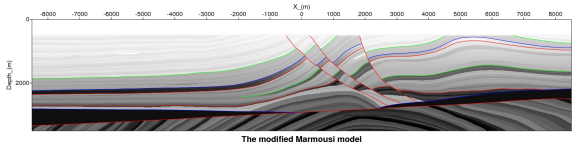

Figure 2: The modified Marmousi model. The modification happened between $x = -6000m$ and $x = -5000m$ where the lateral variation is mild. The low velocity values are boosted to water speed ($1500m/s$). The colored horizons are major reflectors in the model.

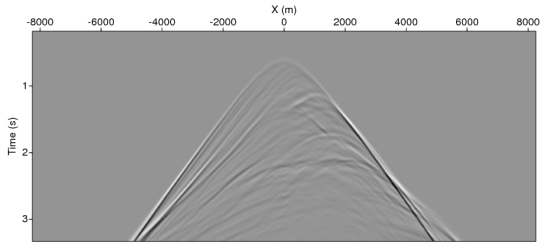

Figure 3: The shot gather with the shot location: $x_s = 0(m)$.

IMAGING RESULTS

The α_1 result for $\theta = 0$ is shown in Figure 4, its corresponding HOIS result is shown in Figure 5. The computational cost from α_1 to $\alpha^{\mathtt{HOIS}}$ is extremely low: 30% of FK migration, but diffractions are not delt with since they are laterally exclusively phenonmena expressed in terms (such as α_{22} and α_{23}).

HOIS results for $\theta = 9^\circ$ (Figure 6) is also shown to demonstrate the fact that: while specular reflections are almost identical for different angle θ, diffractions swings around noticeably for different θ. This is the reason why after summing the HOIS image from all angles (see Figure 8), the specular reflections are boosted and the diffractions are much reduced.

The Marmousi model is the most complicated model we had tested on the inverse scattering based imaging, yet the same dependendable purposefulness of the terms is observed:

1. The common-image gather becomes flat where the correct depth is achieved although the flatness of the common-

image gather does not enter the algorithm. And the bigger the distance from the final image to its actual location, the bigger the curvature of the event in the common-image gather.

2. In the common-image gather the flattening effect is much stronger on specular reflections than on diffractions.

One surprise is that, after summing the imaging results from all angles, the reduction of diffractions is the most effective for the Marmousi experiment compared with all previous models we had tested.

CONCLUSIONS

Testing the current imaging algorithm with partial capture of the direct depth ISS imaging terms demonstrates encouraging results on the Marmousi model data set. HOIS represents only a small fraction of ISS imaging terms. Therefore further ISS terms, for example HOIS+LE (Wang and Weglein, 2010) add further imaging capability that includes terms that only contribute for laterally varying media, and similarly, the laterally exclusive term in α_{23} will be studied and evaluated to incorporate and provide a more effective and capable imaging algorithm. This test is next important milestone on the road for ISS depth imaging toolbox. The promise and potential is to provide an accurate depth image under complex and daunting imaging challenges, where: (1) an adequate velocity cannot be determined and/or (2) the inability to depth image beneath a know and complex velocity model. It will play the same role for depth imaging that inverse scattering free surface and internal multiple removal. They are cut from the same cloth, and will provide differential added value under the same complex and daunting circumstances.

ACKNOWLEDGMENTS

The authors would like to thank all M-OSRP members and sponsors. This work has been partially funded by NSFCMG award DMS-0327778 and DOE Basic Energy Sciences Award DE-FG02-05ER15697. The Marmousi model was downloaded by the first author from the website of the Allied Geophysical Laboratory of University of Houston.

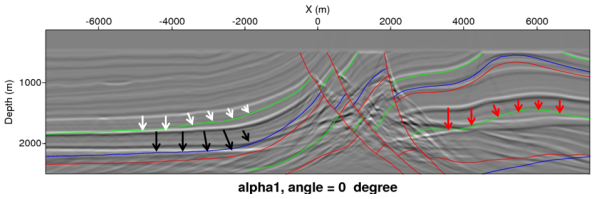

Figure 4: The α_1 imaging result (equivalent with FK migration with $p_h = 0$ or $k_h = 0$). The α_1 result corresponding to equation (2) in this paper and the first and original reference is equation (2.22) of Liu (2006).

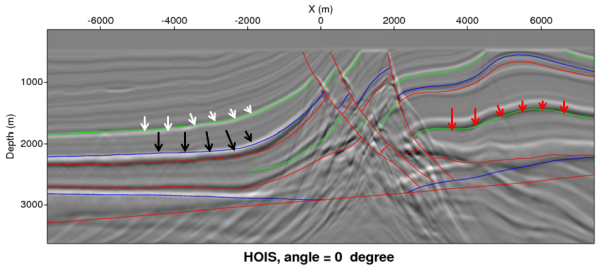

Figure 5: The HOIS imaging result after the calculation of α_1 in Figure 4. The formula to compute this inverse scattering series image is equation (7) of this paper and the first and original reference is equation (2.34) of Liu (2006).

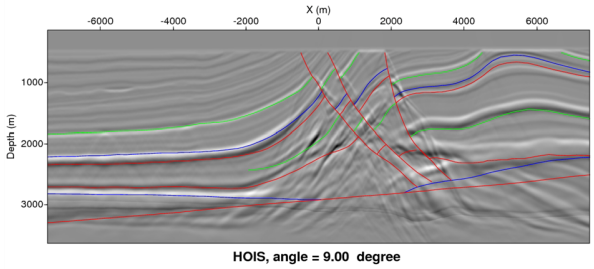

Figure 6: HOIS imaging result for angle $\theta = 9^\circ$.

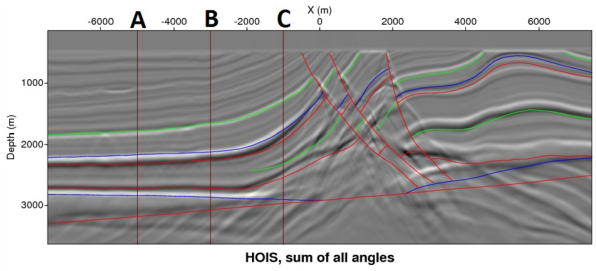

Figure 7: A, B, and C indicate the three locations where the common-image gather analysis in Figure 9 is carried out.

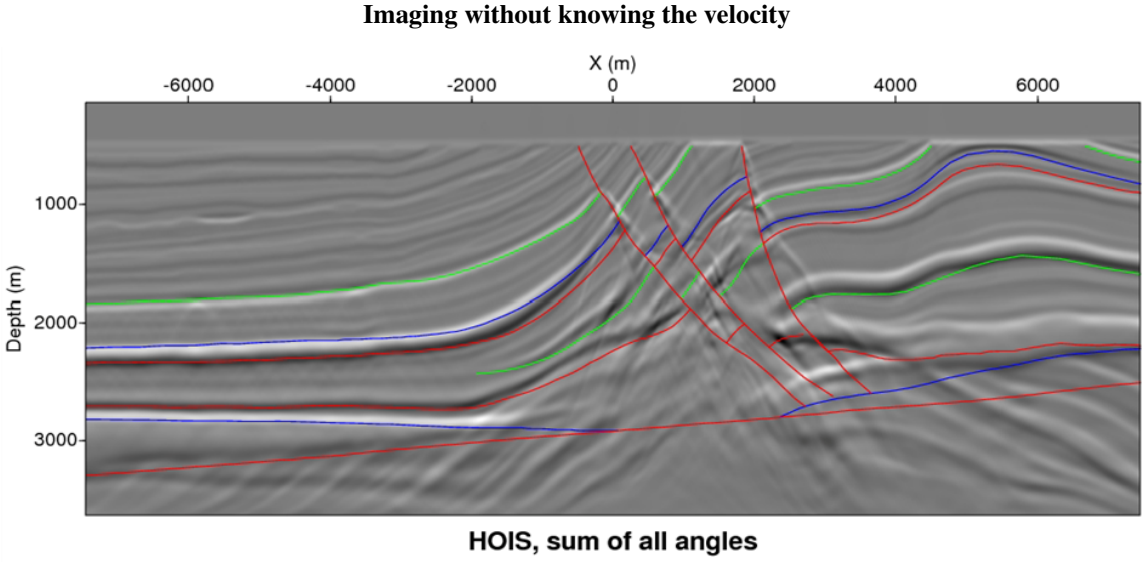

Figure 8: The sum of all HOIS imaging results from all 101 angles between $\theta = 0°$ and $\theta = 9°$.

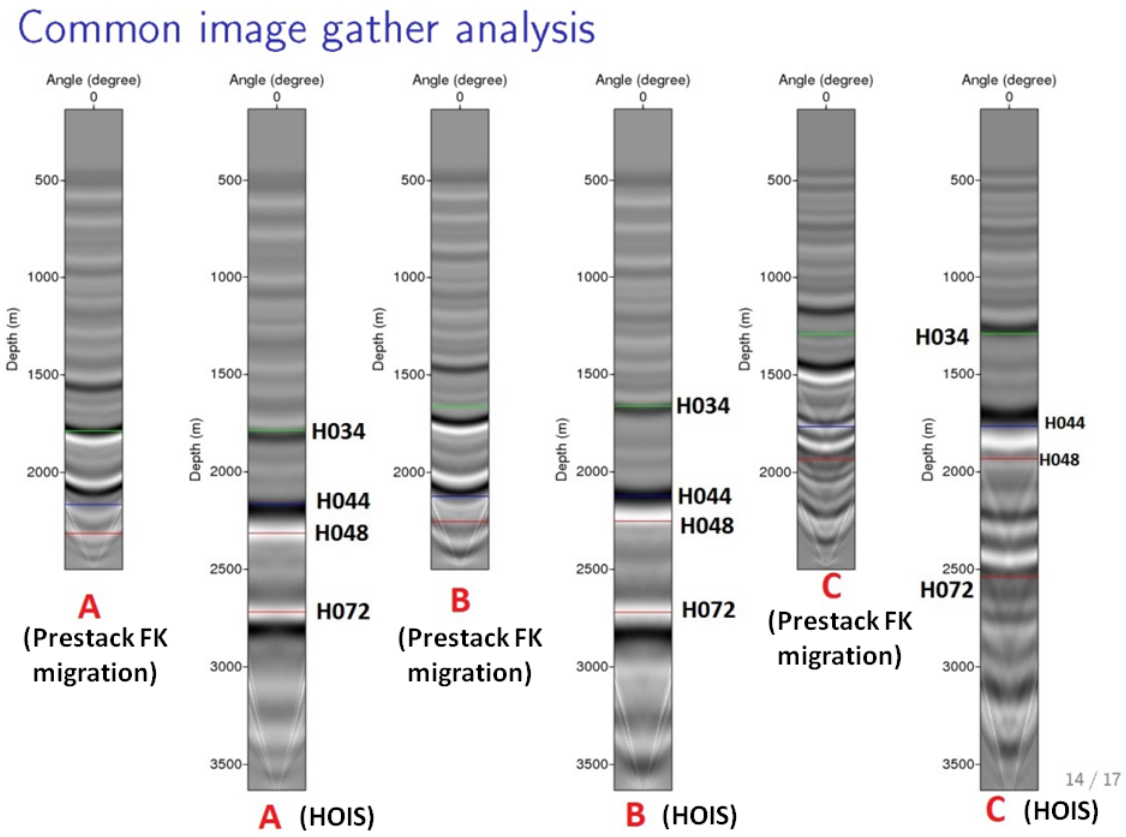

Figure 9: Angle gathers, from left to right: α_1 at location A ($x = -5000(m)$), HOIS at location A; α_1 at location B ($x = -3000(m)$), HOIS at location B; α_1 at location C ($x = -1000(m)$), HOIS at location.

REFERENCES

Liu, F., 2006, Multi-dimensional depth imaging without an adequate velocity model: PhD thesis, University of Houston.

Shaw, S. A., 2005, An inverse scattering series algorithm for depth imaging of reflection data from a layered acoustic medium with an unknown velocity model: PhD thesis, University of Houston.

Wang, Z., and A. B. Weglein, 2010, An investigation of iss imaging algorithms beyond hois, to begin to address exclusively laterally varying imaging challenges: M-OSRP Annual Report, **10**, 105–114.

Weglein, A. B., 2006, Introduction and overview: Mosrp06: M-OSRP Annual Report, **6**, 1–4.

Weglein, A. B., D. J. Foster, K. H. Matson, S. A. Shaw, P. M. Carvalho, and D. Corrigan, 2002, Predicting the correct spatial location of reflectors without knowing or determining the precise medium and wave velocity: initial concept, algorithm and analytic and numerical example: Journal of Seismic Exploration, **10**, 367–382.

Weglein, A. B., F. Liu, X. Li, P. Terenghi, E. Kragh, J. D. Mayhan, Z. Wang, J. Mispel, L. Amundsen, H. Liang, L. Tang, and S. Hsu, 2012, First field data examples of inverse scattering series direct depth imaging without the velocity model, *in* 76th Annual Internat. Mtg., Soc. Expl. Geophys., Expanded Abstracts: Soc. Expl. Geophys., 1–6.

Weglein, A. B., K. H. Matson, D. J. Foster, P. M. Carvalho, D. Corrigan, and S. A. Shaw, 2000, Imaging and inversion at depth without a velocity model: Theory, concepts and initial evaluation, *in* 70th Annual Internat. Mtg., Soc. Expl. Geophys., Expanded Abstracts: Soc. Expl. Geophys., 1016–1019.